

# F-Actin, a Model Polymer for Semiflexible Chains in Dilute, Semidilute, and Liquid Crystalline Solutions

J. Käs,\* H. Strey,† J. X. Tang,\* D. Finger,\* R. Ezzell,§ E. Sackmann,‡ and P. A. Janmey\*

\*Division of Experimental Medicine, Brigham and Women's Hospital, Harvard Medical School, Boston, Massachusetts 02115 USA;  
†Technische Universität München, Physik Department, Biophysics Group, 85748 Garching, Germany; §Surgery Research Laboratory, Massachusetts General Hospital, Department of Surgery, Harvard Medical School, Charlestown, Massachusetts 02129 USA

**ABSTRACT** Single actin filaments were analyzed in solutions ranging from dilute (0.2 µg/ml), where filaments interact only with solvent, to concentrations (4.0 mg/ml) at which F-actin forms a nematic phase. A persistence length of ~1.8 µm and an average length of ~22 µm (Kaufmann et al., 1992) identify actin as a model for studying the dynamics of semiflexible polymers. In dilute solutions the filaments exhibit thermal bending undulations in addition to diffusive motion. At higher semidilute concentrations (1.4 mg/ml) three-dimensional reconstructions of confocal images of fluorescently labeled filaments in a matrix of unlabeled F-actin reveal steric interactions between filaments, which account for the viscoelastic behavior of these solutions. The restricted undulations of these labeled chains reveal the virtual tube formed around a filament by the surrounding actin. The average tube diameter  $\langle a \rangle$  scales with monomer concentration  $c$  as  $\langle a \rangle \propto c^{-(0.5 \pm 0.15)}$ . The diffusion of filaments in semidilute solutions ( $c = (0.1\text{--}2.0)$  mg/ml) is dominated by diffusion along the filament contour (reptation), and constraint release by remodeling of the surrounding filaments is rare. The self-diffusion coefficient  $D_{||}$  along the tube decreases linearly with the chain length for semidilute solutions. For concentrations  $>2.5$  mg/ml a transition occurs from an isotropic entangled phase to a coexistence between isotropic and nematic domains. Analysis of the molecular motions of filaments suggests that the filaments in the aligned domains are in thermal equilibrium and that the diffusion coefficient parallel to the director  $D_{||}$  is nearly independent of filament length. We also report the novel direct observation of u-shaped defects, called hairpins, in the nematic domains.

## INTRODUCTION

Actin filaments (F-actin) play an essential role in cell mechanics (Janmey et al., 1991; Elson, 1988) and cell motility (Stossel, 1993) and are an informative system for the study of the properties of semiflexible polymers (Sackmann, 1994). Actin monomers (G-actin,  $M_r$  42,000) polymerize in physiological salt solutions to form double-stranded helical filaments. In vitro solutions of F-actin have a polydisperse length distribution that depends on the kinetics of polymerization and is altered by the presence of contaminating actin-binding proteins (Casella and Torres, 1994). A typical solution of highly purified actin can have a range of lengths visible by fluorescence microscopy from about 1 µm to 70 µm, with a mean length of ~22 µm (Kaufmann et al., 1992).

Biopolymers such as actin and DNA have become useful systems for the study of fundamental aspects of polymer physics because they have several advantages over synthetic polymers. Bulk properties of synthetic polymers have been extensively analyzed, but even the largest synthetic polymer is too small to observe individually by methods such as light microscopy, which could show directly the dynamics of single chains. Some types of biopolymers, on the other hand, exhibit in vitro a

length of several microns and are easy to visualize by fluorescence labeling. This allows a new approach to polymer physics (Ishijima et al., 1991; Smith et al., 1992; Volkmuth and Austin, 1992; Käs et al., 1994; Perkins et al., 1994) by observing the dynamics of single chains on a millisecond to hour time scale.

Nature provides model polymers for all three stiffness regimes usually distinguished in polymer science—stiff rods, semiflexible polymers, and flexible polymers—as shown in Fig. 1. The semiflexible case seems to be the most suitable for video microscopy. Stiff rods such as microtubules show translational and rotational diffusion, but no internal motions. Flexible polymers such as neurofilaments or DNA (Perkins et al., 1994) exhibit an overlapping random coil configuration, which prevents detection of internal dynamics of the chain unless the chain is stretched out by external forces or, in the case of polyelectrolytes, in low ionic strength by interacting charges. In contrast, the interplay between bending stiffness and entropy provides an extended shape for semiflexible chains such as F-actin, and internal motions are easy to follow in the fluorescence microscope.

In this study, we used fluorescence and video microscopy to visualize single rhodamine-phalloidin-labeled actin filaments in dilute solutions or embedded in semidilute solutions and nematic phases of unlabeled F-actin. This approach allows analysis of the thermally driven motions of individual actin filaments. Analysis of diffusion in semidilute solutions strengthened our previous confirmation (Käs et al., 1994) of the tube model (Edwards, 1967) and the concept of reptation (de Gennes, 1971), which explain the

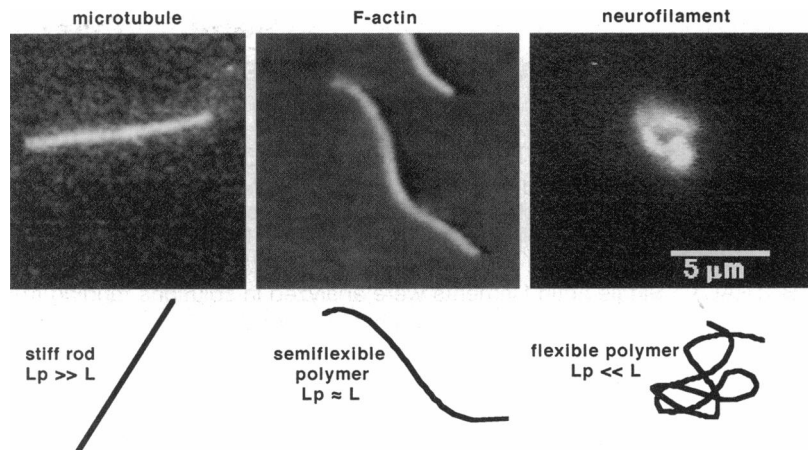
Received for publication 17 May 1995 and in final form 11 October 1995.

Address reprint requests to Dr. J. Käs, Department of Experimental Medicine, LMRC 301, Brigham and Women's Hospital, Harvard Medical School, 221 Longwood Ave., Boston, MA 02115. Tel.: 617-278-0390; Fax: 617-734-2248; E-mail: kas@calvin.bwh.harvard.edu.

© 1996 by the Biophysical Society

0006-3495/96/02/609/17 \$2.00

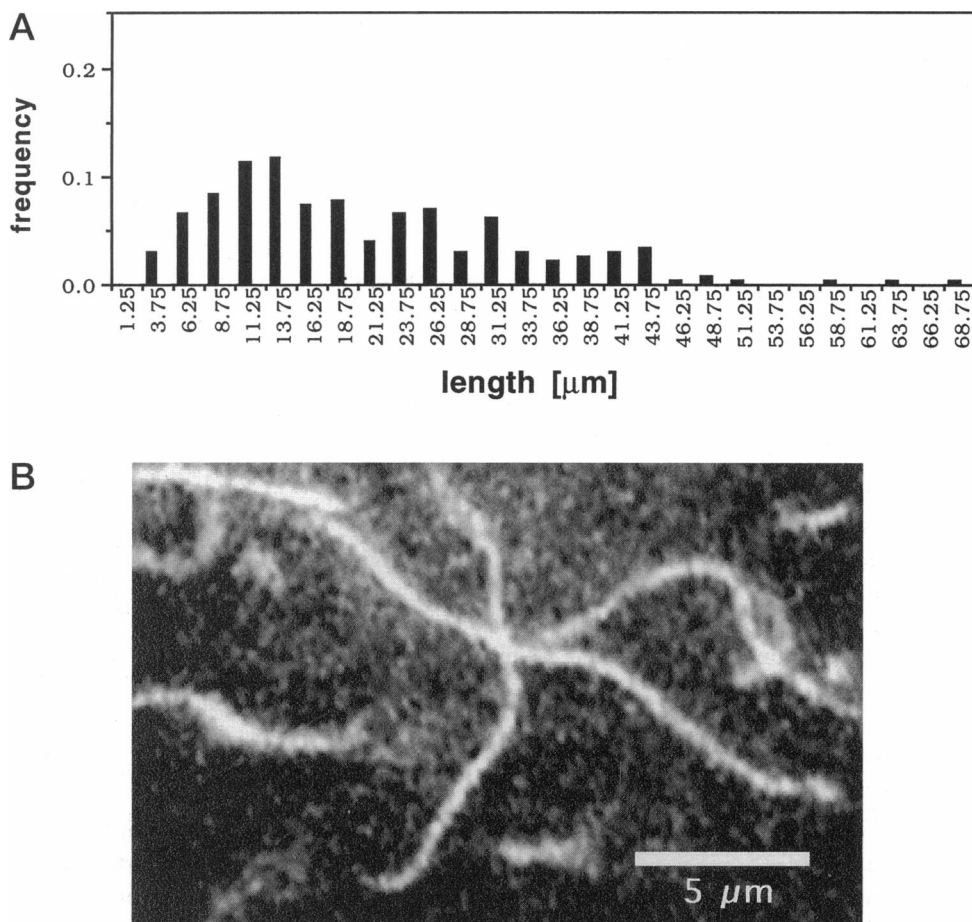
**FIGURE 1** Classification of polymer stiffness by the persistence length  $L_p$ . This concept is based on the idea that the correlation between the orientations of the local tangent  $t(s)$  decays with the distance  $s$  along the filament contour according to  $\langle t(s) \cdot t(s') \rangle = \exp(-|s - s'|/L_p)$ . The rhodamine-labeled microtubule, which has a persistence length  $L_p$  exceeding the filament length  $L$ , is a typical example for a stiff rod. The semiflexible character of the rhodamine-phalloidin-labeled actin filament can be expressed by the fact that  $L_p$  and  $L$  are comparable. In case of flexible polymers, like the rhodamine-labeled neurofilament shown above, a random coiled shape, which is dominated by entropy, can be observed. The high flexibility implies that the persistence length  $L_p$  is smaller than the filament length  $L$ .

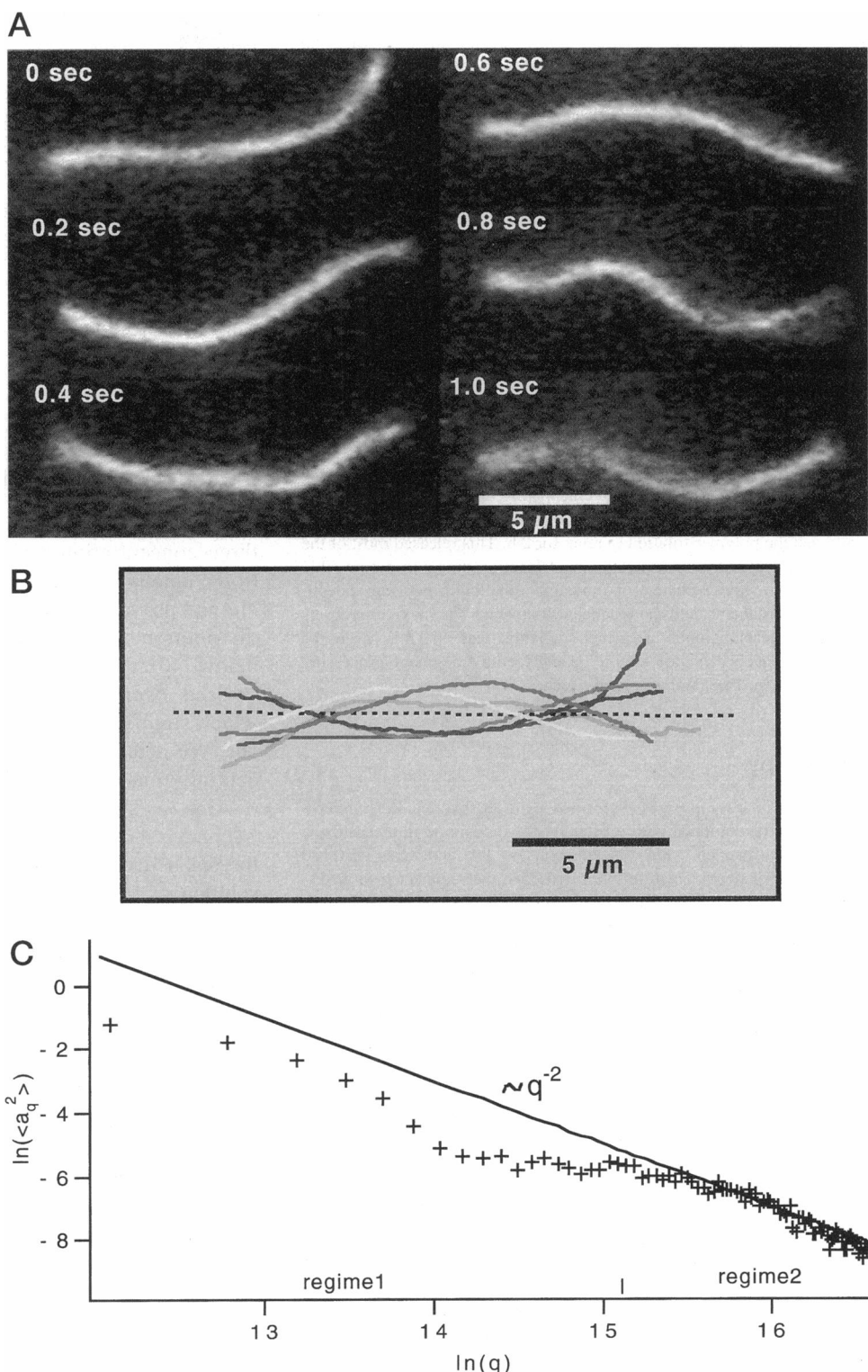


diffusion of a polymer chain in an isotropic solution of entangled polymers. In more concentrated F-actin solutions we observed the filaments in a state of aligned and entangled domains due to a transition from an isotropic phase to a nematic-isotropic coexistence. Formation of aligned domains is predicted by classical theories of stiff polymers (Onsager, 1949; de Gennes and Prost, 1994) and has previously been demonstrated experimentally with F-actin (Suzuki et al., 1991; Coppin and Leavis, 1992; Furukawa et al.,

1993). By visualizing the motions of individual chains within the aligned domains we show that they retain a very high degree of diffusional freedom along the director and therefore are able to attain thermodynamic equilibrium between the isotropic and nematic phases. This first direct observation of the dynamics of semiflexible polymers in a nematic phase also indicated that the chain interactions speed up the diffusion of the filaments and make it nearly independent of filament length.

**FIGURE 2** (a) *In vitro* length distribution of polymerized actin. The filaments show a very broad length distribution of up to 69  $\mu\text{m}$  and an average length of 20  $\mu\text{m}$ . The length distribution was determined with rhodamine-phalloidin-labeled F-actin in the fluorescence microscope. In some of our preparations the maximum length of the filaments dropped to  $\sim 44 \mu\text{m}$  and an average length of 14  $\mu\text{m}$ . (b) Onset concentration of the semidilute regime. In a 40 nM solution of rhodamine-phalloidin-labeled F-actin single filaments start to overlap and sterically restrict each other.





## **EXPERIMENTAL PROCEDURES**

## Sample preparation

Monomeric actin (G-actin) was purified from rabbit skeletal muscle by the method of Spudich and Watt. One preparation was further processed by gel filtration chromatography on a Sephadryl S200 column. We could not detect any differences between the two preparation methods in our experiments.

G-actin was rapidly frozen in liquid N<sub>2</sub> and stored at -80°C. On the day of use aliquots of actin were quickly thawed at 37°C. Actin was polymerized for 2 h at room temperature or for 12 h at 5°C in F-buffer (2 mM Tris, pH 7.5, 0.5 mM ATP or 1.0 mM ATP in the case of the 12-h polymerization time, 0.2 mM CaCl<sub>2</sub>, 150 mM KCl, 2 mM MgCl<sub>2</sub>).

Incorporation of a trace amount of fluorescently labeled polymers into a matrix of unlabeled polymers permits observation of the motion of single

chains in solution with significant polymer-polymer overlap (Käs et al., 1994; Perkins et al., 1994). For this purpose we polymerized two actin solutions: a 5  $\mu\text{M}$  F-actin solution labeled with rhodamine-phalloidin (TRITC-phalloidin; Sigma, St. Louis, MO) at a molar ratio of 1:1, and an unlabeled solution of the desired concentration for the polymer matrix. To adjust the final concentration of the labeled filaments in the sample to 2.5 nM/10 nM (fluorescence microscope/confocal microscope) a small fraction of the labeled solution was pipetted into the unlabeled solution and mixed by repeated pipetting. The pipette tip (1-ml Eppendorf) was cut to a broader diameter (~7 mm), and pipetting was done slowly to prevent filament breakage (Janmey et al., 1994). At higher actin concentrations (due to the higher polymerization rates) we also polymerized the unlabeled matrix around the labeled filaments instead of mixing the two solutions. To reduce bleaching of the fluorescent dye, 4  $\mu\text{g}/\text{ml}$  catalase, 0.1 mg/ml glucose, 20  $\mu\text{g}/\text{ml}$  glucose oxidase, and 0.05 vol % mercaptoethanol were added to the sample, and all solutions used were initially degassed for 30 min.

After mixing, the sample was placed between a glass microscope slide and a cover glass. The slide was sealed with vacuum grease, which also provided a spacing of ~80  $\mu\text{m}$  between the slide and the cover glass. To prevent adsorption of the actin filaments at the glass surfaces we coated the surfaces with monomeric actin by preincubating the cover glass and slide with a 25  $\mu\text{M}$  G-actin solution for ~15 min. After the sample was sealed we allowed the polymer solution to relax for 2 h. This released most of the initial strain caused by mixing. A longer relaxation time was not possible because of the slow exchange of rhodamine-phalloidin between the initially labeled filaments and the unlabeled filaments. The maximum observation time, bleaching under permanent radiation, was ~20 min before the labeled filaments became too faint to be analyzed by the image-processing system. Filament breakage was rarely seen.

## Microscopy

Fluorescence microscopy was performed with an inverted Zeiss microscope (Axiovert) equipped with a filter set for rhodamine fluorescence, a Zeiss Plan Neofluar 63 $\times$  Ph3 objective ( $n\text{A} = 1.4$ ) and Zeiss HBO100 light source. For documentation the microscope was connected to a SIT-camera (SIT68; Dage, Michigan City, IN) by a 4 $\times$  coupler. The images were recorded on videotape by a SVHS recorder.

Confocal microscopy was done using a Biorad MRC 600 Confocal Imaging System (Biorad, Hemel Hempstead, England) attached to a Zeiss Axiovert with a Zeiss Plan Neofluar 100 $\times$  objective ( $n\text{A} = 1.4$ ). Images were obtained in the slow scanning (1 frame/s), photon-counting mode. The interslice distance for a z-series was 0.2  $\mu\text{m}$ . Confocal microscopy of very dilute F-actin was not possible because the image would smear out due to the fast thermal undulations of the filaments and the slow scanning rates of the microscope. However, when the labeled filaments were embedded in a network with a mesh size smaller than the resolution of the microscope (~300 nm), the undulations could not be detected, and a sharp picture could be obtained.

## Image processing

Fluorescence images were digitized by a frame grabber (Pixel Pipeline; Perceptics, Knoxville TN) installed in an Apple Macintosh IIci with an accelerator board (Daystar 33 MHz Turbo40; DayStar Digital, Flowery Branch, GA). Image analysis was carried out with a modified version of the image-processing software Image (Wayne Rasband, National Institutes of Health, Bethesda, MD).

The spatial coordinates of an actin filament were determined using only filaments that were entirely in the focal plane ( $\pm 0.1 \mu\text{m}$ ). The contours of the filaments ( $x(s)$ ,  $y(s)$ ) ( $s$ : arc length) were measured by the following method. First the two ends of the filament were marked interactively to estimate where the tracing algorithm had to stop. Next, a point in the middle of the filament was chosen with the mouse. The intensity profile around this point was used to fit a quadratic test function. The fit was done for a range of different tangent angles, and the angle was chosen for which

the steepness of the intensity profile was the largest. The maximum of the fitted profile was stored as coordinate point. By fitting a test function the positions ( $x(s)$ ,  $y(s)$ ) could be located with an accuracy of  $\pm 11 \text{ nm}$  and was limited only by the signal-to-noise ratio. The determined tangent angle was used to direct the search matrix for the neighboring intensity maximum. The minimum distance for the next maximum between two neighboring pixels is 1.42 times the dimension of a square pixel if the tangent angle is 45°. We used this fact to jump at least one pixel. For this maximum the fitting procedure described above was repeated and the next data point was stored. This procedure was repeated until an intensity drop indicated the end of the filament.

Three-dimensional reconstruction of confocal images was performed using Voxblast software (Unix version, Vaytek) on a Silicon Graphics Indigo2 computer (Silicon Graphics, Mountain View, CA).

## RESULTS

### A mode analysis of the thermally excited bending motions in dilute solutions

F-actin solutions can be characterized by the following three concentration regimes: noninteracting dilute solutions; entangled, semidilute solutions; and concentrated, aligned phases. Solutions of actin filaments of the length distribution shown in Fig. 2 *a* are dilute at concentrations below 40 nM. Above this concentration the solution crossed over from dilute to semidilute conditions in which significant filament-filament overlap begins to occur. We detected this transition by determining the concentration at which rhodamine labeled filaments start to overlap, as shown in Fig. 2 *b*.

Fig. 3 *a* shows a typical time sequence of the unrestricted, thermally driven motions of an actin filament in a dilute solution of labeled F-actin of monomer concentration 2.5 nM. The pictures were taken at time intervals of 0.2 s. On this time scale of a few tenths of a second the filament exhibits bending undulations around a straight mean shape (see Fig. 3 *b*). The freely undulating filament fills a cylindrical space with a maximum diameter of ~5  $\mu\text{m}$ . Besides bending undulations perpendicular to the focal plane the filament remained in focus for a period of 1–2 s. At longer times the filament left the focal plane by rotational and translational diffusion.

In the case of small undulations around a straight shape the total bending energy  $H_{\text{bend}}$  of the filament can be expressed by (Landau and Lifshitz, 1980)

$$H_{\text{bend}} = \frac{k_c}{2} \int_0^L \left( \frac{\partial \vartheta}{\partial s} \right)^2 ds \quad (1)$$

where the integration extends over the filament length  $L$ ,  $k_c$  denotes the bending modulus, and  $\vartheta$  is the tangential angle along the contour.

For a normal-mode analysis of the thermal bending excitations we performed a Fourier decomposition of the tangential angle  $\vartheta(s)$ :

$$\vartheta(s) = \sum_q a_q \cos(qs) \quad (2)$$

where  $q = \pi n/L$  ( $n = 1, 2, 3 \dots$ ) is the wave vector, which corresponds to a wavelength of  $\lambda = \pi/q$ . For free filament ends, the boundary conditions  $(\partial \vartheta/\partial s)_{s=0,L} = 0$  reduce the Fourier expansion for  $\vartheta(s)$  to a cosine expansion.

Using the equipartition theorem we obtained for the mean bending energy of each mode

$$\begin{aligned}\langle H_{\text{bend}}(q) \rangle &= \frac{k_c}{2} \left\langle \int_0^L \left( \frac{\partial}{\partial s} a_q \cos(qs) \right)^2 ds \right\rangle \\ &= \frac{k_c}{4} L q^2 \langle a_q^2 \rangle = \frac{k_B T}{2}\end{aligned}\quad (3)$$

By solving this equation we derive the following equation for the mean square amplitudes  $\langle a_q^2 \rangle$ :

$$\langle a_q^2 \rangle = \frac{2k_B T}{k_c L q^2} \quad (4)$$

This result implies that the mean square amplitudes  $\langle a_q^2 \rangle$  scale with the wave vector  $q$  as  $\langle a_q^2 \rangle \sim q^{-2}$ . Unfortunately, we had to confine the filaments in a narrow space ( $\sim 5 \mu\text{m}$ ) between two glass slides. Otherwise the filament did not stay long enough in the focal plane to sample enough configurations to calculate the mean square value of the amplitudes  $a_q$ . Fig. 3 c shows a typical double logarithmic plot of  $\langle a_q^2 \rangle$  versus  $q$ . For the short wavelength regime the plot shows the expected scaling behavior with a scaling coefficient of  $-2.03 \pm 0.07$ . But for long wavelengths (larger than  $\sim 1 \mu\text{m}$ )  $\langle a_q^2 \rangle$  scales with a lower power of  $q$ . This result shows that the excited modes in this wave vector regime are not only free bending motions. The mode spectra could be changed by tensions restricting the undulations or the influence of other excited motions. Furthermore, we checked for Gaussian distribution of the Fourier amplitudes  $a_q$  by testing if the condition  $\langle a_q^4 \rangle / \langle a_q^2 \rangle^2 = 3$  is fulfilled in the studied wave vector regime. In the low wave vector regime,  $q < 5 \times 10^6 \text{ m}^{-1}$ , the value of  $\langle a_q^4 \rangle / \langle a_q^2 \rangle^2$  is systematically below 3, and improving the statistics by doubling the number of traced filaments (from 100 to 200) does not change this result. For higher  $q$ -values we obtained  $\langle a_q^4 \rangle / \langle a_q^2 \rangle^2 = 3 \pm 0.5$ , proving the expected Gaussian character for bending undulations.

The persistence length  $L_p$ , which can be expressed in terms of the bending modulus  $k_c$  by the formula  $L_p = k_B T/k_c$ , can be calculated by Eq. 4. The average persistence length in the high wave vector regime ( $5 \times 10^6 \text{ m}^{-1} < q < 12 \times 10^6 \text{ m}^{-1}$ ) is  $L_p = 1.8 \pm 0.3 \mu\text{m}$ . This result is in agreement with our previous measurements by end-to-end distance measurements in semidilute solutions (Käs et al., 1994). In the low wave vector regime the persistence length shows a large variance as a function of the wave vector and exhibits a local maximum around  $q = 2 \times 10^6 \text{ m}^{-1}$ . The values for the persistence length are consistently higher in this regime, which re-

sults in a mean value of  $L_p \approx 10 \pm 5 \mu\text{m}$ . The fact that the persistence length is no longer constant for  $q < 5 \times 10^6 \text{ m}^{-1}$  expresses again our observation that in the long wave length regime other modes besides bending motions are excited and are not suitable for calculating the bending modulus.

## Entanglements of F-actin in semidilute solutions

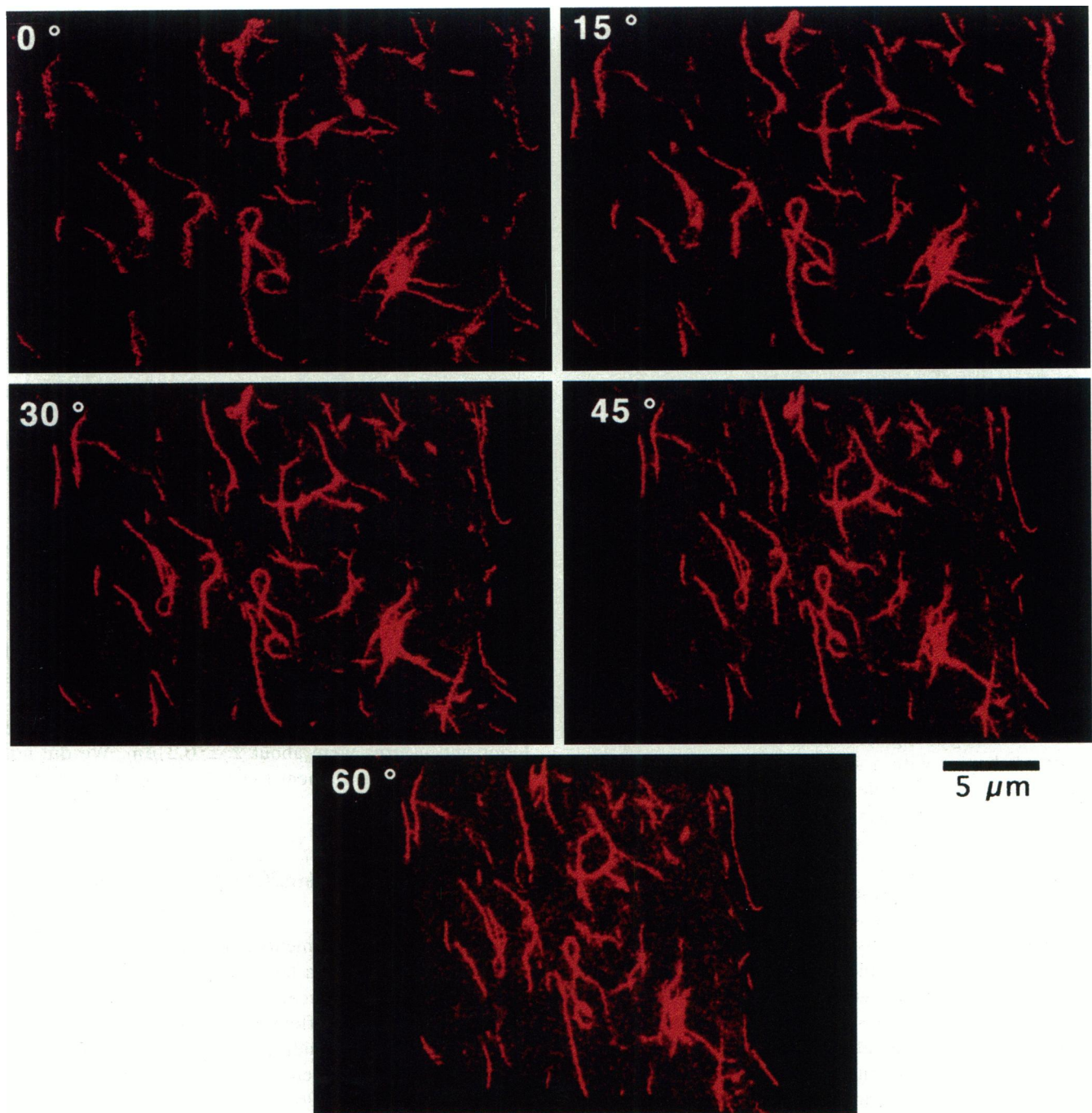
Semidilute F-actin solutions have length-dependent viscoelastic properties, and solutions of very long filaments can have shear moduli of several hundred pascals at low volume fractions over a wide frequency range of exciting shear oscillations (Janmey et al., 1994; Müller, 1991). This shear resistance is caused by the highly entangled state of long actin filaments. To study the structure of these entanglements we embedded labeled filaments in a matrix of unlabeled filaments at a ratio of 1:3500 and examined the entanglement of the labeled filaments by confocal microscopy.

Fig. 4 displays a three-dimensional reconstruction of a partially labeled entangled network rotated 60° about the  $z$  axis. The actin solution ( $c = 1.4 \text{ mg/ml}$ ) contains  $\sim 2.32 \times 10^{12} \text{ filaments/ml}$ , assuming an average filament length of  $22 \mu\text{m}$  and the ratio of labeled to unlabeled filaments is 1:3300. The fluorescently labeled filaments form u-turns and single loops around neighboring filaments. The smallest radii of curvature we found for these loops and u-turns were about  $2 \pm 0.2 \mu\text{m}$ . We did not observe any actin filament twisted into knots or around each other.

## Restricted bending undulations in semidilute F-actin solutions

Rhodamine-labeled filaments embedded in semidilute F-actin solutions exhibit a large drop in the amplitudes of bending oscillations because of filament-filament contacts (see Fig. 5). For flexible chains these steric interactions with the surrounding chains were described as a tube around the filament formed by the surrounding polymers (Edwards, 1967). This idea also applies for semiflexible filaments with the modification that the finite bending stiffness of the filaments creates a characteristic minimum length between two points where the filament touches the tube (Odijk, 1983). This distance is called the deflection length.

The thermal undulations of the filament visible by microscopy define the tube diameter. By superimposing a sufficient number of transient traces of a filament ( $\sim 64$  traces were taken at time intervals of 0.1 s), the tube can be imaged and its diameter measured as the maximum deflection along the contour. Fig. 5 confirms that the restrictions to the thermal undulations of a polymer chain in a polymer solution can be described by a surrounding tube. This description is valid within a concentration



**FIGURE 4** Entangled mesh of actin filaments. To image the network, fluorescently labeled filaments were embedded in a matrix of unlabeled filaments (actin monomer concentration  $c = 1.4 \text{ mg/ml}$ ; ratio of unlabeled to labeled actin, 3300:1). The three-dimensional reconstruction was obtained from a z-series of confocal images of a volume of  $30 \mu\text{m}$  length  $\times 18 \mu\text{m}$  height  $\times 4 \mu\text{m}$  depth, and the sequence shows a total rotation of  $60^\circ$ .

range of  $0.1 \text{ mg/ml}$  to  $4.0 \text{ mg/ml}$  (including the coexistence regime between nematic and isotropic domains). At lower concentrations this concept breaks down because of the increasing role of constraint release, as we show below (see Fig. 9). The gray line in Fig. 5 shows a snapshot of the undulating chain within the tube. For the filament shown in Fig. 5 we estimated the deflection

length  $\lambda_d$  at  $\lambda_d \approx 3.8 \pm 0.6 \mu\text{m}$  by measuring the average distance between two contact points of transient contours of the filament ( $n = 10$ ) with the tube.

The mean diameter  $\langle a \rangle$  of a tube was determined by averaging its diameter measured at  $0.5\text{-}\mu\text{m}$  intervals along the tube axis. Table 1 summarizes the results for the mean tube diameter,  $\langle a \rangle$ , and for the variation of the tube diameter

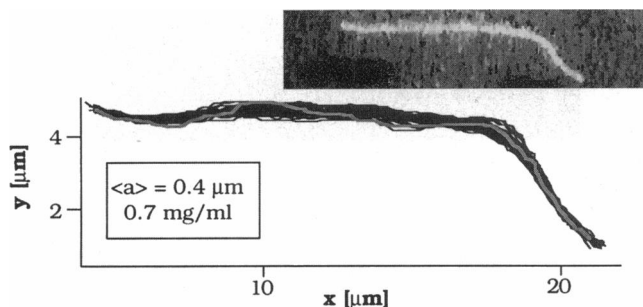


**FIGURE 5** Direct visualization of a tube around an actin filament in a solution of 0.7 mg/ml F-actin. The picture was obtained by superimposition of 64 traces of the contour taken at time intervals of 0.1 s. The insert above the graph displays a snapshot of the filament, which was confined in the tube. Below the tube the mean tube diameter  $\langle a \rangle$  and the actin concentration of the surrounding F-actin matrix are denoted. The gray line shows a snapshot of the undulating chain within the tube and illustrates the concept of a deflection length.

as a function of actin concentration,  $c$ . The  $\langle a \rangle$  values of Table 1 represent the mean value obtained from four filaments per concentration. The mean diameter decreases with increasing concentration from 0.9  $\mu\text{m}$  for a monomer concentration of 0.1 mg/ml to 0.3  $\mu\text{m}$  for  $c = 1.4$  mg/ml. The diameter has a large standard variation, which decreases with increasing  $c$ .

### Diffusion of single actin filaments in semidilute F-actin solutions

Fig. 5 shows that actin filaments remain in their original tube for periods of a few seconds. At longer times the filament was driven out of the tube by its thermal undulations. This results in reptation, a snake-like motion through the entangled mesh (de Gennes, 1971; Doi and Edwards, 1986).

The reptation motion of two labeled filaments of different length in a matrix of unlabeled filaments (of 0.1 mg/ml or 2.0 mg/ml, respectively) is shown in Fig. 6 a. To guide the eye, thin white lines are drawn around the filaments to symbolize a tube with approximately 3–4 times the diameter of the tubes surrounding the filaments.

**TABLE 1** Summary of the mean tube diameter measurements

Actin concentration $c_A$ (mg/ml)	Tube diameter $\langle a \rangle$ ( $\mu\text{m}$ )	$\Delta a/\langle a \rangle$ (%)
0.1	0.94	28
0.4	0.71	26
0.5	0.79	22
0.7	0.43	33
1.4	0.30	13
4.0 nematic domain	0.10	6
4.0 entangled domain	0.13	9

The mean tube diameter  $\langle a \rangle$  decreases with increasing actin concerning  $c$  and shows a large variation  $\Delta a/\langle a \rangle$ , which is typical for the semidilute regime.

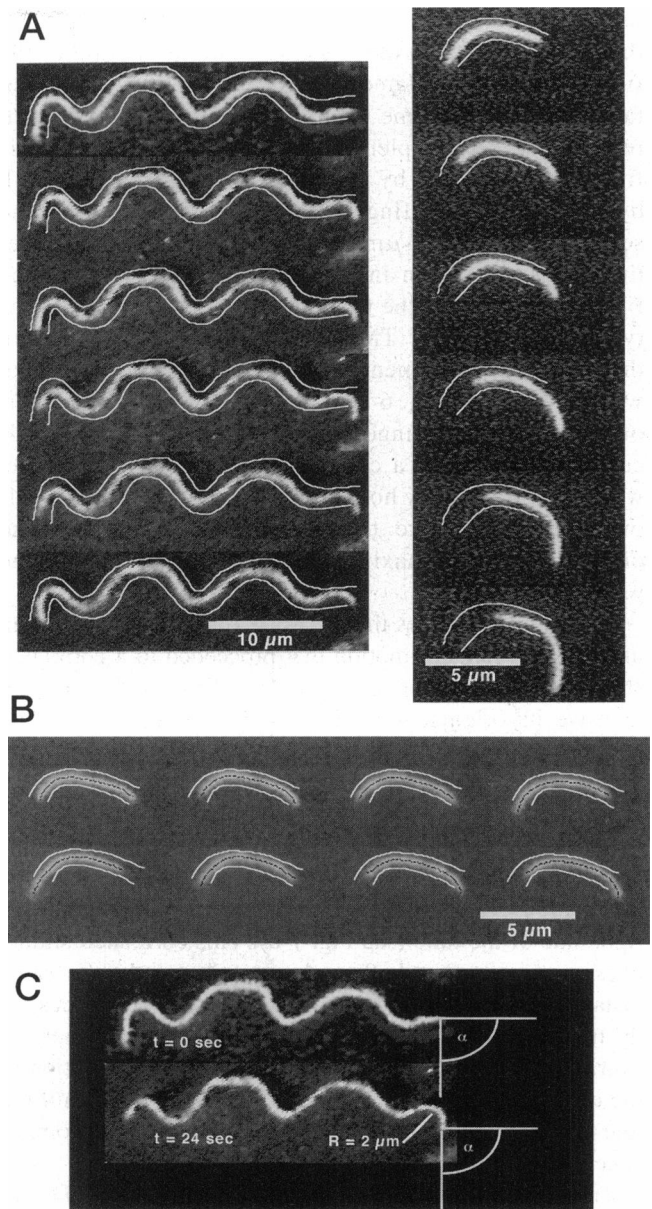


**FIGURE 6** (a) Time sequences ( $\Delta t = 8$  s) of the reptation motion of actin filaments of 40.0  $\mu\text{m}$  (right side) and 6.9  $\mu\text{m}$  length (left side) in a matrix of F-actin of 0.1 mg/ml or 2.0 mg/ml, respectively. The tubes formed by the thin white lines drawn to guide the eye are three to four times larger than the mean diameter of the tube. The shorter filament diffuses visibly faster than the long one. The reptation time is 2.0 min for the short filament and 61.4 min for the long filament. (b) Time sequence of the reptating filament shown on the right side of (a) recorded at intervals of 1 s. The thin white lines symbolize the surrounding tube, and the black dashed lines along the filament show the traced contour. The shorter time intervals show that the filament slides back and forward to leave its original tube. (c) The minimal radius of curvature  $R$  that a filament end can assume during its thermally driven fingering motions is about 2  $\mu\text{m}$ . The reptation behavior of the left filament of  $a$  gives an example of such radii of curvature.

In a time span of 48 s the filament of 40  $\mu\text{m}$  length explored new tube segments by its fingering motion out of the tube. At first the filament slid  $\sim 3$   $\mu\text{m}$  out of the

tube at the right side. Then it retracted  $\sim 2 \mu\text{m}$  back into the tube. Aside from the correlated sliding motion of the filament ends the filament remained within the original tube. In the same time frame the  $\sim 7\text{-}\mu\text{m}$ -long filament reptated almost completely out of its original tube. This filament left its tube by repeatedly sliding back and forth by the same type of fingering motion as seen in the time sequence for the  $40\text{-}\mu\text{m}$ -long filament but on a shorter time scale, as shown in Fig. 6 b. The amplitude of the fingering motion of the filament ends out of the tube was typically  $\sim 1\text{--}2 \mu\text{m}$ . The minimum radius of curvature that a reptating filament end of this length could make was  $\sim 2 \mu\text{m}$  (see Fig. 6 c). Therefore, the accessible part of the mesh for the fingering motion of the filament ends can be described as a cone around the end of the tube, which is restricted by how far a filament could bend itself over a length where the filament fingers out of the original tube. The maximum opening angle of this cone was  $\sim 90^\circ$ .

On short time scales the ends of a filament performed an uncorrelated random motion that proceeded to a correlated sliding motion on longer time scales, allowing the filament to leave its original tube. This is illustrated in Fig. 7 by recording the motion of the filament ends of the  $40.0\text{-}\mu\text{m}$ -long filament displayed in Fig. 6 in time steps of  $0.12 \text{ s}$  (Fig. 7 a) and  $0.84 \text{ s}$  (Fig. 7 b). In a time interval of  $2.5 \text{ s}$  the ends moved in uncorrelated fashion and in different directions (see Fig. 7 a). In a longer time span of  $34.4 \text{ s}$  we observed a transition to a correlated sliding of the filament out of the right side of the tube (see Fig. 7 b). This correlated sliding does not mean that both ends moved exactly the same distance. The elastic undulating filament does not necessarily transmit the whole motion of one end to the other; on average the motion of the ends is coupled to the motion of the center of mass of the filament because of the semiflexible character of the chain and its low longitudinal compliance.

The diffusion coefficient of a chain along the tube  $D_{\parallel}$  was determined by measuring the diffusive motions of the filament ends for time scales where the motions were correlated. The chain end positions  $(x_i, y_i)$ , with respect to a local coordinate system with  $y_i$  axes parallel to the tube axes at the ends, were recorded at time intervals  $\Delta t = 8 \text{ s}$ . The diffusion coefficient of the ends parallel to the tube is calculated as

$$D_{\parallel} = 1/(N - 1) \sum_{j=2}^N \{(y_i(j) - y_i(j - 1))/(2\Delta t)\}$$

where  $N$  is the number of steps, and in most measurements  $N = 30$ .  $D_{\parallel}$  is the arithmetic mean of the diffusion coefficients of the filament ends  $D_i$  of four independent time sequences ( $30 \times 8 \text{ s}$ ). The results of our measurements are summarized in the graph of Fig. 8.  $D_{\parallel}$  decreases linearly with increasing chain length  $L$ . Within experimental error we did not detect any dependence on the monomer concen-

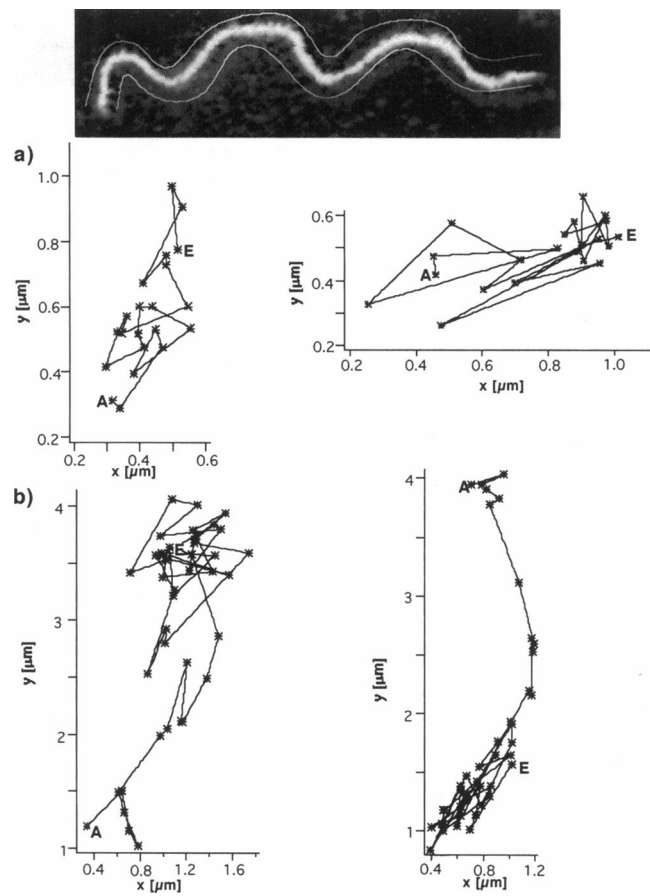


FIGURE 7 Track of the movement of filament ends of the filament displayed on the left side of Fig. 6 a in steps of  $0.12 \text{ s}$  (a) and  $0.84 \text{ s}$  (b), respectively. The y-axes are oriented parallel to the local axes of the tube at the two ends. Each time sequence starts at point A and ends at point E.

tration  $c$  within a concentration range of  $c = (0.1\text{--}2.0) \text{ mg/ml}$ .

The reptation time  $\tau_D$  is defined as the time a chain needs to leave its original tube entirely. The reptation time can be calculated from the diffusion coefficient of a chain along the tube  $D_{\parallel}$  by  $\tau_D = L^2/D_{\parallel}/\pi^2$  (Doi and Edwards, 1986). This equation applies for flexible chains. The reptation time, which has been predicted for wormlike chains, is practically the same (Keep and Pecora, 1985). The results of this calculation are listed in Table 2. The calculated reptation time increases from  $2.2 \text{ min}$  for the filament of  $6.9 \mu\text{m}$  length displayed in Fig. 6 to  $15 \text{ h } 36 \text{ min}$  for a filament of  $50.5 \mu\text{m}$  length. The calculated value of  $\tau_D$  for the  $6.9\text{-}\mu\text{m}$ -long filament agrees with the value of  $2.0 \text{ min}$  we obtained for  $\tau_D$  by direct observation (Fig. 6).

Because all filaments are able to diffuse in the solution, a filament can leave its original tube not only by its own reptation motion, but the structure of the tube can change if chains of the surrounding polymer matrix reptate away. This process is called constraint release (Lodge et al., 1990). In the concentration range of  $0.1\text{--}2.0 \text{ mg/ml}$  constraint release was a very infrequent event because of the tightly packed

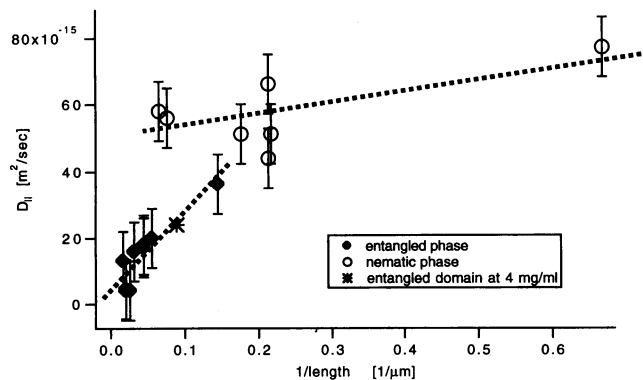


FIGURE 8 Length dependence of the diffusion coefficient  $D_{\parallel}$ . In the pure entangled phase the diffusion coefficient along the tube increases linearly with the inverse filament length. The measured diffusion coefficient of the filament in the entangled domain at 4 mg/ml indicates that this scaling behavior also applies for the entangled phase in the coexistence regime. The diffusion coefficient  $D_{\parallel}$  parallel to the director in the nematic domains at 4 mg/ml is nearly length independent and shows a large variance. The error bars were calculated from the statistical error among the four independent time sequences that were used to obtain the average.

meshwork. In a solution of semiflexible chains the tube changes its shape because of constraint release only if the change in the mesh exceeds the persistence length. At lower concentrations of  $\sim 0.01$  mg/ml constraint release began to dominate the diffusion in the loose mesh of filaments. Fig. 9 illustrates that at higher actin concentrations diffusion of filaments was determined by reptation and that the tube model breaks down at low concentrations. At 0.4 mg/ml the

TABLE 2 Summary of the measured diffusion coefficient  $D_{\parallel}$  and the resulting reptation time  $\tau_D$  that a filament needs to leave its original tube

Actin concentration $c_A$ (mg/ml)	Filament length $L$ ( $\mu\text{m}$ )	Diffusion coefficient $D_{\parallel}$ ( $\text{m}^2/\text{s}$ )	Reptation time $\tau_D = L^2/\pi^2 D_{\parallel}$
0.1	22.7 $\mu\text{m}$	$1.7 \times 10^{-14}$	51.1 min
	40.0 $\mu\text{m}$	$4.4 \times 10^{-14}$	61.4 min
0.4	22.7 $\mu\text{m}$	$1.8 \times 10^{-14}$	48.3 min
	59.5 $\mu\text{m}$	$1.3 \times 10^{-14}$	7 h 42 min
0.5	50.5 $\mu\text{m}$	$4.6 \times 10^{-15}$	15 h 36 min
	50.5 $\mu\text{m}$	$2.0 \times 10^{-15}$	28.0 min
0.7	18.2 $\mu\text{m}$	$1.6 \times 10^{-14}$	109.4 min
	32.2 $\mu\text{m}$	$4.3 \times 10^{-15}$	17 h 48 min
1.4	52.1 $\mu\text{m}$	$3.6 \times 10^{-14}$	2.2 min
2.0	6.9 $\mu\text{m}$	$7.7 \times 10^{-14}$	3.0 s
4.0	4.6 $\mu\text{m}$	$5.1 \times 10^{-14}$	42.0 s
	4.7 $\mu\text{m}$	$4.4 \times 10^{-14}$	50.6 s
	4.7 $\mu\text{m}$	$6.6 \times 10^{-14}$	33.9 s
	5.7 $\mu\text{m}$	$5.1 \times 10^{-14}$	64.5 s
	13.3 $\mu\text{m}$	$5.6 \times 10^{-14}$	5.3 min
	15.7 $\mu\text{m}$	$5.8 \times 10^{-14}$	7.2 min
	11.2 $\mu\text{m}$	$2.4 \times 10^{-14}$	8.8 min

The first space in the table separates the data below 2.5 mg/ml from the data at 4.0 mg/ml in a nematic domain. The last value in the table is for a filament in an entangled domain at 4.0 mg/ml.

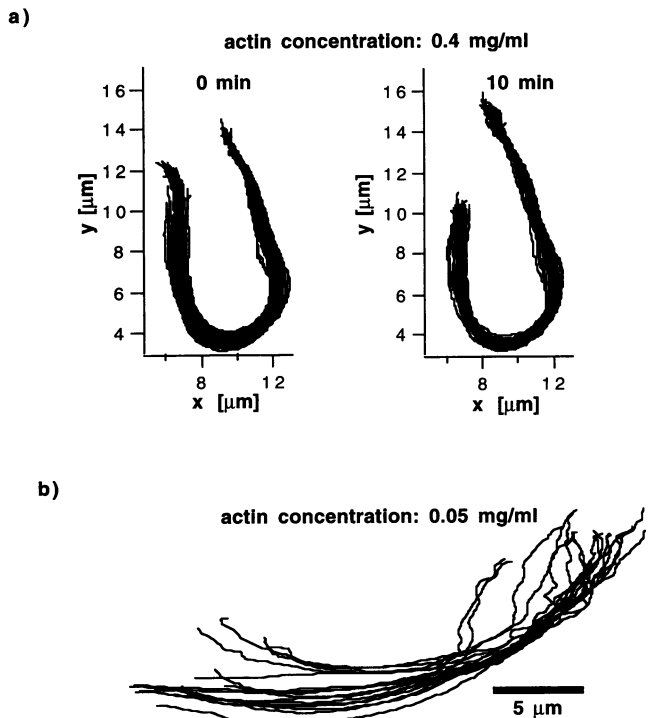
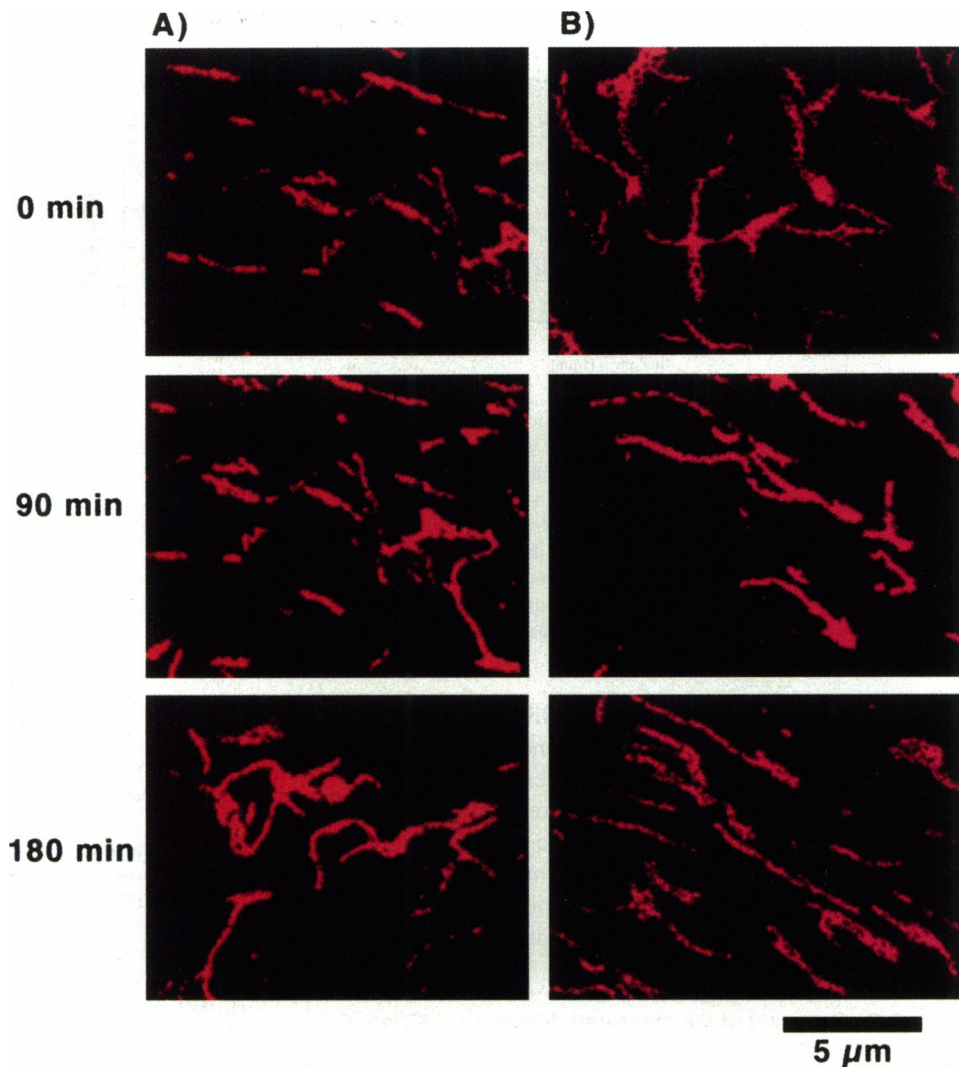


FIGURE 9 Validity of the tube model. (a) Development of the tube around a filament at a concentration of 0.4 mg/ml. The contour of the tube was obtained in the same way as described above. After 10 min the filament left the original tube at both ends by repeatedly sliding backward and forward, which can be seen by the changes in the contour of the tube at both ends. The central part of the tube remains unchanged because the mesh is too dense for constraint release to occur. (b) Thirty transient contours taken at time intervals of 2 s at a lower concentration ( $c = 0.05$  mg/ml). The steric interactions can no longer be described as a tube. Constraint release now plays a major role.

F-actin solution formed a tight mesh of  $\sim 0.7$   $\mu\text{m}$  mesh size, and the tube around the filament changed its contour mostly at its ends, because the filament was only able to leave its original position by reptation (see Fig. 9 a). In more dilute solutions ( $c = 0.05$  mg/ml) the concept of a tube surrounding a filament became invalid. The mesh was so loose that rotational diffusion started to be an important contribution and the constraining filaments diffused away within several minutes.

### Alignment of filaments at higher actin concentrations

It has been reported that F-actin solutions undergo a transition to a nematic phase above actin concentrations of 2.0 mg/ml (Suzuki et al., 1991; Coppin and Leavis, 1992; Furukawa et al., 1993). The alignment of filaments, which has been detected by birefringence and anisotropic light scattering, is characteristic for this liquid crystalline phase. In a true nematic phase, as distinct from a bundle of actin filaments, aligned filaments should be able to diffuse along



**FIGURE 10** Relaxation of actin filaments from nonequilibrium states. (A) Relaxation of a shear aligned F-actin solution (1.4 mg/ml) into an isotropic entangled phase. (B) Relaxation of a F-actin solution (4.0 mg/ml) from an entangled, nonequilibrium state into a nematic domain. Confocal pictures were taken at 0 min, 1.5 h, and 3 h.

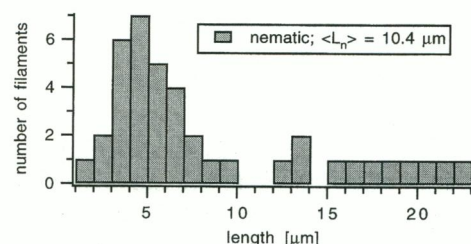
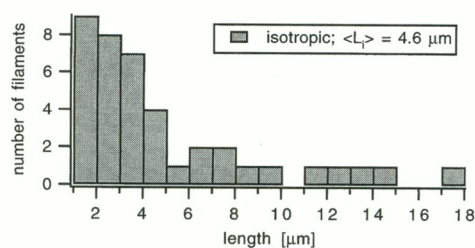
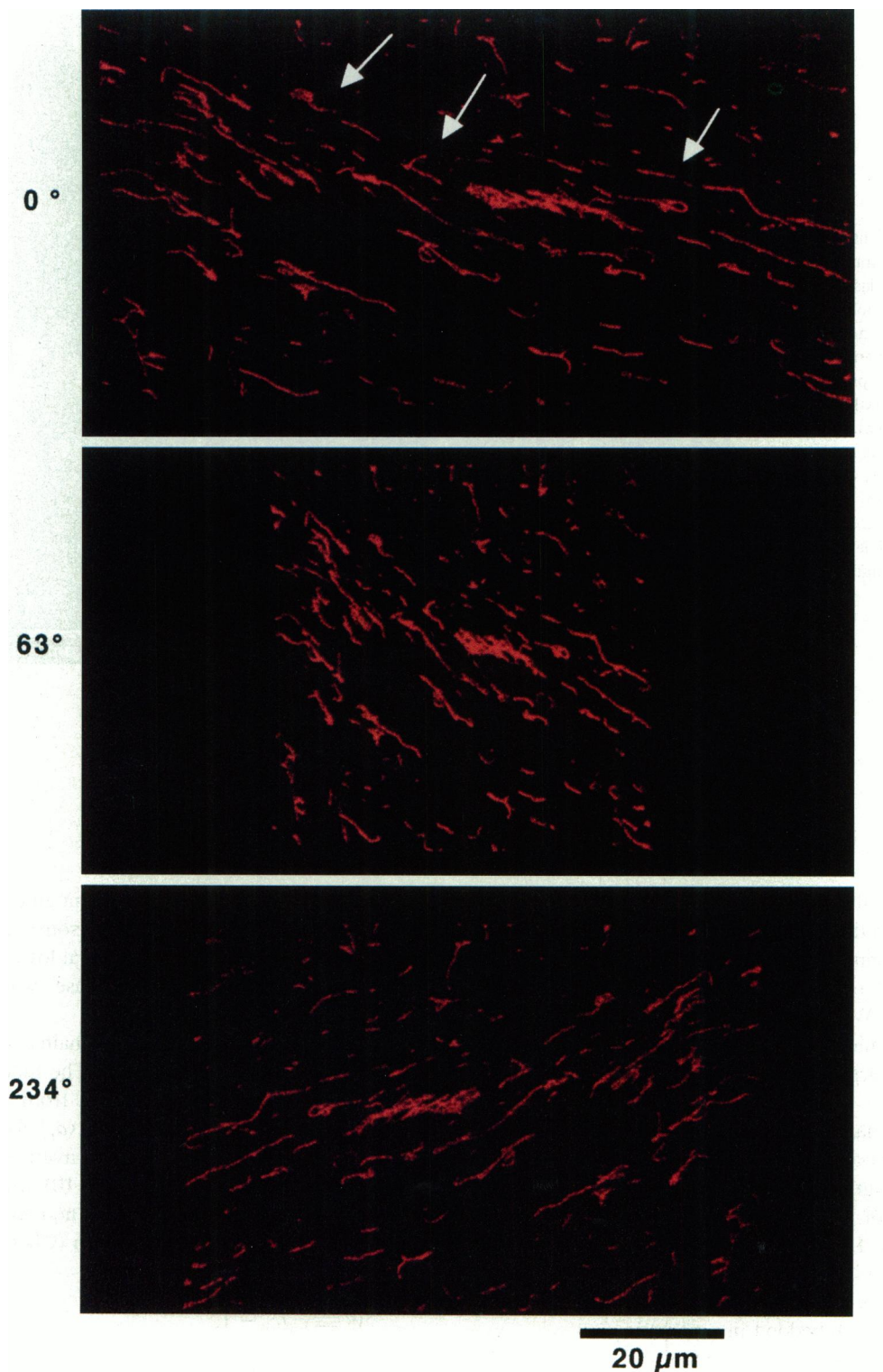
the axis of alignment, which is called the direction of the director, as in a fluid.

Alignment of actin filaments begins to occur at 1.4–2.0 mg/ml, shortly after the actin solution is pipetted onto the cover glass. This nonequilibrium state is caused by the high sensitivity of actin filaments to shear alignment. After 2–3 h the filaments relax into an isotropic entangled network (Fig. 10 A). At concentrations higher than 2.5 mg/ml the aligned areas in the F-actin solutions remain stable and some of the initially isotropic regions of entangled filaments align within 1.5–2 h (see Fig. 10 B). The actin solution used in this experiment was characterized by a maximum filament length of 44  $\mu\text{m}$  and an average length of 14  $\mu\text{m}$ .

Solutions of F-actin of concentration  $\geq 2.5$  mg/ml show clear birefringence between crossed polarizers and remain birefringent for more than 2 weeks. The solutions exhibit a very broad coexistence between the isotropic and the nematic phase. At concentrations from 2.5 to 6.0 mg/ml we always found a mixture of aligned and entangled domains of a size of about 60  $\mu\text{m}$  to 140  $\mu\text{m}$ . A total demixing into purely aligned and isotropic phases did not occur, even after 1 week. Only after spinning the samples in a tabletop centrifuge for several hours did total phase separation take place.

Fig. 11 a shows a three-dimensional reconstruction of one of the aligned domains displayed at different angles.

**FIGURE 11** (a) Three-dimensional reconstruction of an aligned domain of actin filaments at 4.0 mg/ml. The micrographs show different views of a cube of 110  $\mu\text{m}$  length  $\times$  60  $\mu\text{m}$  height  $\times$  5  $\mu\text{m}$  depth. The white arrows mark the phase boundary with an entangled domain. The fluorescently labeled filaments align along the axis of the director. The picture also indicates that the longer filaments are preferentially in the nematic domains. (b) Length distribution of rhodamine-phalloidin-labeled actin filaments in the nematic and isotropic domains at an actin monomer concentration of 4.0 mg/ml. The maximum length is 17  $\mu\text{m}$  and the average length  $\langle L_i \rangle = 4.6 \mu\text{m}$  in the isotropic phase. In the nematic phase the maximal length is 22  $\mu\text{m}$  and the average length  $\langle L_n \rangle$  is 10.4  $\mu\text{m}$ .



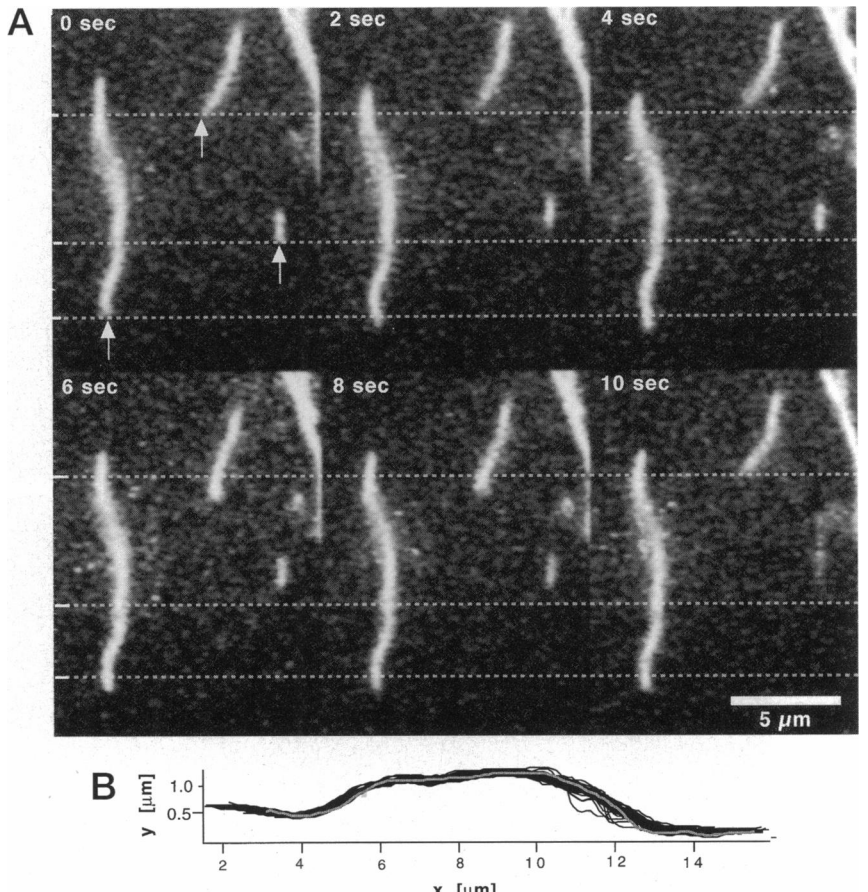


**FIGURE 12** (a) Diffusion of actin filaments in a nematic domain (actin monomer concentration  $c = 4.0 \text{ mg/ml}$ ). The white arrows and dashed lines ( $y$ -coordinate) mark the original position of the diffusing filaments. The filaments move along the axis of alignment. The small filament on the right side diffused out of the focal plane after 10 s without changing its orientation (which we checked by focusing through the sample). (b) Tube-like free space around the long filament of *a* (left side) in a nematic domain. The tube is very narrow and has a mean diameter of 104 nm. The fluctuations in the diameter are very small. The gray line shows a snapshot of the undulating chain within the tube. The deflection length is  $\sim 4.5 \mu\text{m}$ .

Despite the parallel orientation of the filaments, this image also demonstrates imperfections in the alignment, indicating a low-order parameter. The filaments exhibited bends away from the axis of alignment and even u-turns—so-called hairpins (de Gennes, 1982; Williams and Warner, 1990)—as deviations from their main orientation. The formation and appearance of these hairpins will be discussed in detail below.

Longer filaments were found mainly within the nematic domains, whereas short filaments accumulated in the isotropic phase. To illustrate this length-dependent phase separation we measured the length of 40 filaments, each in a nematic and an isotropic domain. The results are shown in Fig. 11 *b*.

The time sequence of Fig. 12 *a* illustrates diffusion of three filaments of different lengths embedded in a nematic domain of a 4.0 mg/ml F-actin solution. The filaments slid quickly back and forth along the axis of the director, and the short filament suddenly disappeared out of the focal plane without first changing its orientation. As long as the filaments were oriented parallel to the director they diffused as in a viscous fluid. The diffusion coefficient parallel to the director of the nematic domains  $D_{\parallel}$  was measured by the method described above, and the results are summarized in Fig. 8.  $D_{\parallel}$  is nearly length independent and, for the longest filaments, higher than the diffusion coefficient along the

tube in the entangled phase. The diffusion coefficient along the tube measured for a filament in a coexisting isotropic domain was in agreement with the values measured at lower concentrations in which only the isotropic phase was formed.

The free space around a filament in a nematic domain can also be pictured as a tube, as shown in Fig. 12 *b*. The tube was very narrow and showed very little variation from a mean diameter of 104 nm. The average diameter  $\langle a_n \rangle$  for four filaments was  $(100 \pm 10)$  nm, whereas the average diameter in the entangled domains  $\langle a_i \rangle$  was  $(130 \pm 10)$  nm. The relative density difference of the isotropic and nematic phases  $W$  can be defined by the following equation (Chen, 1993):

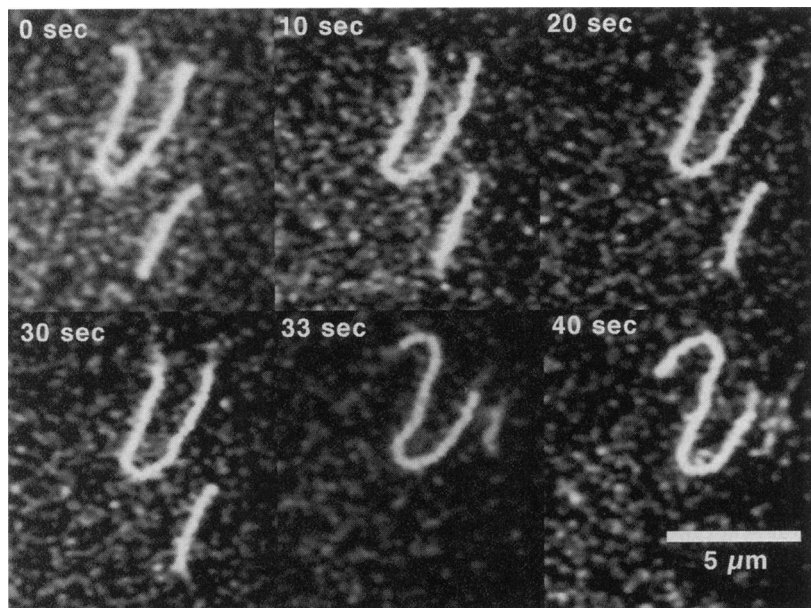
$$W \equiv c_n/c_i - 1, \quad (5)$$

where  $c_n$  is the number of filaments per volume in the nematic phase and  $c_i$  is the number in the isotropic phase. Assuming that filament end effects can be neglected we estimate the relative density difference by

$$W \equiv c_n/c_i - 1 \approx \langle a_i \rangle^2/\langle a_n \rangle^2 - 1, \quad (6)$$

where  $\langle a_i \rangle$ ,  $\langle a_n \rangle$  are the mean tube diameter in the isotropic and nematic phase. The difference in the diameters implied a filament density difference of 60% between the nematic

**FIGURE 13** Formation of a hairpin in a nematic domain ( $c = 4.0 \text{ mg/ml}$ ). In addition to the existing hairpin, a second one formed by the fingering motion of the left filament end. The sliding seems to be slower than for straight filaments. The smaller filament to the right of the filament with the hairpins diffused out of the focal plane at the end of the time sequence.



and the isotropic phase. Equation 6 is just an estimate based on the simplified assumption that the volume per filament can be described by a cylinder with diameter  $\langle a \rangle$ .

The formation of a u-shaped defect, called a hairpin, is shown in Fig. 13. The filament slid repeatedly in both directions of the director and the left filament end fingered nearly perpendicular to the director. After several tries the filament end suddenly flipped over in the other direction and a hairpin formed. The generation of a second hairpin along the same filament was a very infrequent event.

## DISCUSSION

Fluorescently labeled actin filaments represent a versatile system for the study of semiflexible polymers in a wide concentration range from dilute solutions to concentrated, nematic solutions. The data obtained from this study provide a better understanding of F-actin solutions *in vitro* and therefore allow better predictions for the function of actin filaments in cells. The main conclusions that may relate to actin function *in vivo* are that purified actin filaments do not display specific chemical interactions with each other, but can form viscoelastic networks because of steric interactions. The transition from isotropic to nematic structures that occurs over a small concentration range may also be relevant to the formation of such structures as filopodia and stress fibers. Although it seems unlikely that phases attain thermodynamic equilibrium in cells, the thermodynamic drive to form aligned domains and the surprising motility of filaments within such domains may act in concert with specific actin-binding proteins to produce the variety of actin bundles observed *in vivo*.

### Dilute solution dynamics

In dilute solutions polymer chains exhibit unrestricted internal motions. The visible motions of a filament are dom-

inated by bending undulations. The motions occur around a straight mean shape, which confirms the semiflexible character of F-actin. This also means that the filaments exhibit no spontaneous curvatures caused by defects under these conditions. Kinks such as we have recently observed (Käs et al., 1993) did not appear in the presence of compounds used to reduce photobleaching of the sample.

For short wavelengths the mode spectrum of the filament is dominated by bending modes, as expected for wormlike chains (Doi and Edwards, 1986). In the long-wavelength regime they exhibit a different scaling behavior than for pure bending motions. This could be due to the confinement between two glass plates (Hendricks et al., 1995), which could restrict the long modes. Coupling of the bending modes to other modes could also cause deviations from the expected scaling behavior. A third possibility is that Eq. 4, which has been derived for small undulations, does not apply to the long-wavelength regime, where the description that bending undulations have only a component perpendicular to the filament axis may no longer be a valid approximation.

The general character of F-actin as a semiflexible polymer was observed at all concentration ranges tested, but there were significant differences between the apparent filament stiffness in the dilute and semidilute regimes. Free actin filaments in dilute solution show only small bends, and the persistence length we determined by end-to-end distance measurements is about one order of magnitude higher than the value we determined previously in semidilute solutions (Käs et al., 1994). This finding indicates that the persistence length is comparable to the length of the filament ( $\sim 22 \mu\text{m}$ ) and disagrees with our finding of a persistence length of  $1.8 \mu\text{m}$  measured by an analysis of the thermal undulations. It is also inconsistent with the observation that a reptating filament shows minimum radii of curvature of  $\sim 2 \mu\text{m}$ , implying a persistence length of a few microns. We con-

clude that the free filaments show an apparent increased stiffness, possibly due to coupling of the bending modes to other modes such as torsion (Prochniewicz et al., 1995), a restricted sliding motion of the strands of a filament against each other (Bremer et al., 1991), or a partial untwisting of the two strands. Unfortunately we are not able to detect motions like these in the fluorescence microscope, because the fluorescence intensity profile of an actin filament has a thickness of  $\sim 0.5 \mu\text{m}$ , which is  $\sim 100$  times the real diameter of the filament. The Debye screening length is  $\sim 1 \text{ nm}$  under the typical buffer conditions for a F-actin solution. The short screening length rules out stiffening and long-range electrostatic interactions for actin filaments. This unexpected behavior of a semiflexible chain is potentially interesting and can be further investigated, for example, by scattering techniques like dynamic light scattering and neutron scattering. A good estimate for the stiffness of F-actin is also important for determining whether a polymerizing actin could deform a cell membrane by a thermal ratchet-like mechanism (Mogilner and Oster, 1995).

### Semidilute solutions and filament-filament contact

The crossover to the semidilute regime, where the filaments start to interact sterically, occurs at  $\sim 40 \text{ nM}$ . By modeling the polymer solution as a solution of stiff rods (Doi, 1975) we obtain for the onset concentration of the semidilute regime  $c^*$

$$c^* = B(M_p/N_A)(1/L^3), \quad (7)$$

where  $M_p$  is the molecular weight of the polymer,  $L$  is the chain length, and  $B$  is a numerical constant for which Doi predicts  $B = 1$ . Using the average chain length of  $22 \mu\text{m}$  in Eq. 7 results in an onset concentration of  $1.3 \text{ nM}$ . More recent computer simulations showed that  $B \approx 30-70$  (Magda et al., 1986). Our experimental value is in good agreement with the predictions by Magda et al. and other data obtained by rheological experiments (Janmey et al., 1986).

The three-dimensional reconstruction of the actin filament matrix (Fig. 4) shows that gel-like elasticity of F-actin can exist in the absence of specific cross-links or even tightly bent entanglements characteristic of flexible polymer networks. Doi estimated that the number of rods  $N$  enveloping a test rod within a distance  $b$  is (Doi, 1975)

$$N \approx bL^2\rho, \quad (8)$$

where  $\rho$  is the number of filaments per volume and  $L$  the filament length. For an actin solution of  $1.4 \text{ mg/ml}$ ,  $b = 300 \text{ nm}$  ( $\equiv$  average tube diameter), and  $\rho = 2.33 \times 10^{12}/\text{ml}$ . A filament of  $L = 22 \mu\text{m}$  will be surrounded by  $\sim 300$  filaments, which contact it by invading the tube containing the test filament. Even though each contact may be fleeting, their numbers ensure that the filament is kept confined within the tube, just as it would be if it were chemically

linked to the other filaments, at least on a time scale shorter than the reptation time (50 min).

The stiffness of the chains is reflected by a characteristic distance between two points where the filament is able to touch the tube. We measured a deflection length of  $3.8 \mu\text{m}$  for a tube with a diameter of  $400 \text{ nm}$ . Theoretical considerations predict the following dependence of the deflection length  $\lambda_d$  on the mean tube diameter  $\langle a \rangle$  and the persistence length  $L_p \approx 1.8 \mu\text{m}$  (Odijk, 1983):

$$\lambda_d = \langle a \rangle^{2/3} L_p^{1/3}. \quad (9)$$

By using Eq. 9 we calculated a deflection length of  $0.7 \mu\text{m}$ . This is considerably smaller than the measured value. This means that our measurements overestimate the deflection length or  $L_p \gg 1.8 \mu\text{m}$ . We favor the first possibility because we only detect contact points of the chain with the tube in the  $xy$  plane. Bends of the filament in the  $z$  direction within a tube of  $400 \text{ nm}$  diameter are only visible as a broadening of the intensity profile and cannot be identified as contact points.

The fact that concentration fluctuations are characteristic for the semidilute regime is reflected in the large variation of the tube diameter. Despite the variation of the diameter, Table 1 shows that the mean diameter  $\langle a \rangle$  decreases with increasing actin monomer concentration  $c$ . Semenov has pointed out that the tube which an undulating semiflexible chain probes is smaller than the mesh size  $\xi$  of the network because the chains can only bend to a certain degree (Semenov, 1986; Graessley, 1980). This can be expressed by the following formula:

$$\langle a \rangle \sim \xi(\xi/L_p)^{1/5}, \quad (10)$$

where  $L_p$  is the persistence length. Assuming that we can approximately describe the concentration dependency of the mesh size by a scaling law for stiff rods,  $\xi \approx c^{-1/2}$  (de Gennes et al., 1976), we obtain the following equation:

$$\langle a \rangle \sim c^{-3/5}. \quad (11)$$

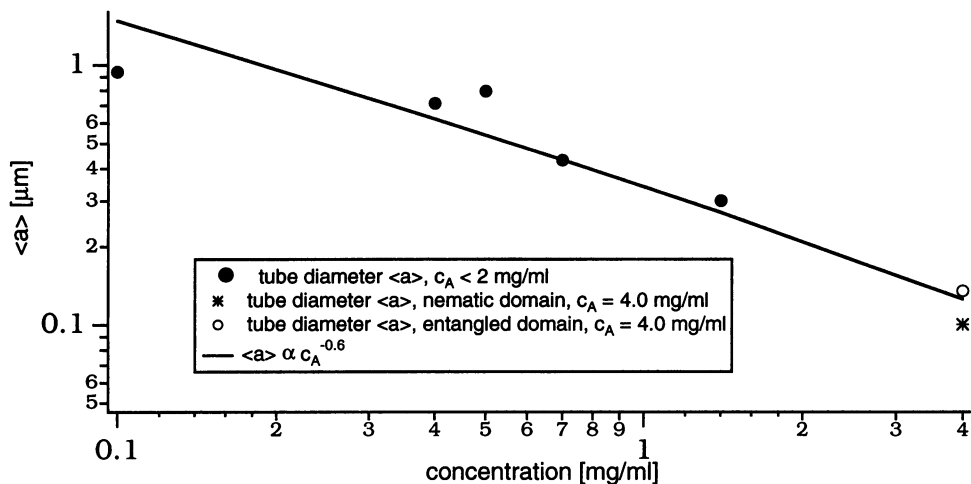
The five values we obtained from Table 1 are not sufficient to establish the scaling law we predicted in Eq. 11. But the plot in Fig. 14 at least shows that our data are in good agreement with Eq. 11. Previous mesh size measurements of F-actin are also consistent with these data (Schmidt et al., 1989).

The scaling argument we derive also agrees with predictions by Odijk, which can be expressed by the following formula (Odijk, 1983):

$$\rho \langle a \rangle^{5/3} L_p^{1/3} L \gg 1, \quad (12)$$

where  $\rho$  is the filament density and  $L$  the filament length. Assuming an average filament length of  $22 \mu\text{m}$  we obtain a filament density of  $2.33 \times 10^{12}$  filaments/ml for an actin monomer concentration of  $1.4 \text{ mg/ml}$ , and an average tube diameter larger than  $14 \text{ nm}$  according to Eq. 12.

FIGURE 14 Mean tube diameter  $\langle a \rangle$  as a function of the actin monomer concentration  $c$ . Below 2 mg/ml the mean tube diameter scales approximately as  $\langle a \rangle \propto c^{-3/5}$ . For 4.0 mg/ml the average tube diameter is 130 nm in the entangled domains and 100 nm in the nematic domains.



### Reptation within a tube

Figs. 6 and 7 confirm that the diffusion of actin filaments in F-actin solutions can be described by the reptation model, which has been developed for flexible chains (de Gennes, 1971; Edwards, 1967) and was later modified for semiflexible, so-called wormlike chains (Odijk, 1983). On short time scales the filament is confined in its tube. Our results prove Odijk's wormlike tube model (Odijk, 1983) and show that other models—like the fuzzy cylinder model (Sato et al., 1991)—do not apply. At longer times the filament ends explore new tube segments, and finally the filament slides out of its original tube, driven by its thermal undulations. The speed of this motion depends critically on the length of the filament. Fig. 6 shows how a filament reptates out of its original tube. A characteristic feature of this motion is the crossover from a random motion of the filament ends to a correlated sliding out of the tube. Theories of polymer physics often refer to the random part of this motion as tube fluctuations (Doi and Edwards, 1986). The crossover occurs sooner for the shorter filaments.

Ignoring minor corrections that arise from the length dependence of the friction coefficient  $\zeta$ , the diffusion coefficient along the tube  $D_{\parallel}$  is predicted to increase linearly with inverse filament length  $L$  in isotropic suspensions (Doi and Edwards, 1986):

$$D_{\parallel} = (k_B T) / (\zeta L) \quad (13)$$

The data for filaments in the entangled phase shown in Fig. 8 confirm the prediction of Eq. 13. The slightly lower values for the measured diffusion coefficient in comparison to our previously published values can be explained by the change of the time interval between two measured positions of the filament ends from 0.12 s to 8 s. In case of the short time interval we have included uncorrelated motions of the filament ends in the calculation of the diffusion coefficient along the tube  $D_{\parallel}$ , which did not contribute to the motion of the entire filament, and virtually increased the measured value. It is expected that hydrodynamic effects cause devi-

tions from the linear length dependence of  $D_{\parallel}$  and that hydrodynamic screening slows the diffusion down with increasing actin concentration (Muthukumar and Edwards, 1983; Odijk, 1986). Both effects are weak and are not detectable within our experimental error of  $\pm 10 \times 10^{-15}$  m<sup>2</sup>/s and within the small accessible concentration and length regime.

A detailed theory for the diffusion coefficient  $D_{\parallel}$  of a reptating polymer only exists for stiff rods and flexible polymers (Doi and Edwards, 1986). Assuming that the semiflexible actin filaments are closer to the case of stiff rods we compare our data with the formula predicted for stiff rods:

$$D_{\parallel} = (k_B T \ln(L/b)) / (2\pi\eta L),$$

where  $b = 7$  nm is the diameter of the filament and  $\eta \approx \eta_{\text{water}}$  is the viscosity of the buffer. The experimental values were smaller by a factor of  $\sim 20$  than the values calculated for stiff rods, indicating that semiflexible chains diffuse more slowly in semidilute solutions. This finding contradicts a theoretical estimate (Doi, 1975) which concludes that semiflexible chains reptate faster than stiff rods in an isotropic phase.

### Constraint release and terminal relaxation time

Above 0.1 mg/ml constraint release within a F-actin network can be neglected, and the diffusion of filaments is dominated by reptation. Even if one of the surrounding chains reptates away, the filament is too stiff to bend enough to fill up the new space and leave its original tube. Only in a very loose mesh where the mesh size is bigger than the persistence length does constraint release play a significant role.

In rheological experiments the crossover from fluid to elastic behavior defines the terminal relaxation time of an F-actin solution under shear (Ruddies et al., 1993; Ferry, 1980). Assuming that this relaxation process is dominated

by reptation we can conclude for a polymer solution with monodisperse length distribution that this time is equal to the reptation time of the polymer chains. According to Ruddies et al. the terminal relaxation time of an F-actin solution is  $\sim 160$  min. Assuming a similar length distribution of the F-actin solutions used in this experiment, this result indicates that the relaxation of shear in a solution of actin filaments is dominated by filaments that are longer than the average filament length. The reptation time, which we calculated from our measurements of the diffusion coefficients, is  $\sim 50$  min for a filament of average length.

### Liquid crystalline phase

Alignment of F-actin by itself does not necessarily result from a thermal equilibrium state representing a nematic phase. A frozen glass-like state of shear-aligned filaments would be also birefringent over long time periods. The time sequences of Fig. 10 show that metastable aligned or entangled domains relax on a time scale of several hours. This result is in agreement with the reptation times we calculated (Table 2; the maximum filament length in the F-actin solution used for the experiments shown in Fig. 10 was  $44\ \mu\text{m}$ ).

The technique of fluorescence imaging of single filaments allows for the first time measurements of the dynamics of polymer chains in a liquid crystalline phase. As expected for polymers in a nematic phase the actin filaments stayed aligned when they diffused. They could only move parallel or perpendicular to their axis. In the nematic phase the diffusion coefficient  $D_{||}$  is enhanced for chains of the same length, because of the decreased entanglements due to the alignment.

Surprisingly, the diffusion coefficient parallel to the director seems to be length independent. One might expect that the diffusion coefficient scales as it does in the isotropic phase, which is in first order inversely proportional to filament length. Recently Radzhovsky and Frey (1993) presented a theory for the hydrodynamics of flux lines in superconductors, which also applies to aligned polymer melts if the Rouse behavior of single chains is replaced by Zimm dynamics. Whereas for noninteracting chains the diffusion coefficient scales with  $1/L$ , the relaxations in the interacting aligned phase are independent of the filament length  $L$ . In the interacting theory the  $1/L$  dependence of the diffusion coefficient is suppressed by the interaction between the chains with increasing filament density. The chain interactions even speed up the dynamics of the chains. If these findings also apply to longitudinal diffusion they could explain the weak length dependence and the increased diffusion coefficients compared to the isotropic phase. To prove that this theory really applies to our experiments, further experiments at different filament densities are required.

We detected a relative density difference of  $60 \pm 15\%$  between the isotropic domains and the nematic domains at a monomer concentration of  $4.0\ \text{mg/ml}$ . Theoretical calcu-

lations for semiflexible polymers predict a density difference of  $\sim 7\%$  at the onset of the coexistence regime (Chen, 1993; Vroege and Odijk, 1988). Interestingly, the relative concentration difference nearly gets length independent for length-to-persistence length ratios larger than 1 (Chen, 1993). The experimental value clearly exceeds the theoretical value. But taking into consideration that in polydisperse systems the relative density difference is expected to be bigger (Vroege and Lekkerkerker, 1992) and that the actin concentration ( $4\ \text{mg/ml}$ ) is nearly double the onset concentration ( $2\ \text{mg/ml}$ ) (Furukawa et al., 1993), for nematic ordering a larger density difference seems to be reasonable. We further observed an enrichment of long filaments in the nematic phase (see Fig. 11 b), as expected (Vroege and Lekkerkerker, 1992). This can be explained by the earlier nematic onset concentration for longer filaments.

For lyotropic liquid crystals hairpin-like defects have been predicted by Khokhlov and Semenov (1982). A more refined model by Vroege and Odijk confirmed this prediction (Vroege and Odijk, 1988). We provide a direct visualization of the dynamics of this metastable state (Williams and Warner, 1990). In agreement with theory (Williams and Warner, 1990), the diffusion of a filament exhibiting or forming a hairpin shows two types of motion: i) a reptation-like motion of the chain along its end and ii) a rapid reversal in direction to form hairpins. The strong curvature of the hairpins and the distance between two hairpins ( $\sim 5\ \mu\text{m}$ ) in Fig. 13 agree with our experimental value of  $1.8\ \mu\text{m}$  for the persistence length. Vroege and Odijk predicted that the typical distance between hairpins is about 3.25 times the persistence length.

We are grateful for discussions with T. Duke, S. Fraden, E. Frey, P. G. de Gennes, K. Kroy, S. Leibler, D. Nelson, G. Oster, J. Prost, P. van der Schoot, and T. P. Stossel. We thank J. F. Leterrier and R. Vegners for providing the fluorescently labeled neurofilaments. We also thank C. Cunningham for help and advice.

This work was funded by a Forschungsstipendium of the Deutsche Forschungsgemeinschaft (JK), by National Institutes of Health Grant AR38910 (JK, PAJ), SFB 266 (ES), and the American Cancer Society (RE).

### REFERENCES

- Bremer, A., R. C. Millonig, R. Sutterlin, A. Engel, T. D. Pollard, and U. Aebi. 1991. The structural basis for the intrinsic disorder of the actin filament: the "lateral slipping" model. *J. Cell Biol.* 115:689–703.
- Casella, J. F., and M. A. Torres. 1994. Interaction of Cap Z with actin. The NH<sub>2</sub>-terminal domains of the alpha 1 and beta subunits are not required for actin capping, and alpha 1 beta and alpha 2 beta heterodimers bind differentially to actin. *J. Biol. Chem.* 269:6992–6998.
- Chen, Z. Y. 1993. Nematic ordering in semiflexible polymer chains. *Macromolecules*. 26:3419–3423.
- Coppin, C. M., and P. C. Leaviss. 1992. Quantitation of liquid-crystalline ordering in F-actin solutions. *Biophys. J.* 63:794–807.
- de Gennes, P. G. 1971. Reptation of a polymer chain in the presence of fixed obstacles. *J. Chem. Phys.* 55:572–579.
- de Gennes, P. G. 1982. In *Polymer Liquid Crystals*. A. Ciferri, W. R. Krigbaum, and R. B. Meyer, editors. Academic, New York. Chapter 5.

- de Gennes, P. G., P. Pincus, R. M. Velasco, and F. Brochard. 1976. Remarks on polyelectrolyte conformation. *J. Physiol. (Paris)*. 37: 1461–1473.
- de Gennes, P. G., and J. Prost. 1994. *The Physics of Liquid Crystals*. Clarendon, Oxford.
- Doi, M. 1975. Rotational relaxation time of rigid rod-like macromolecule in concentrated solution. *J. Physiol. (Paris)*. 36:607–617.
- Doi, M. 1985. Effect of chain flexibility on the dynamics of rodlike polymers in the entangled state. *J. Polym. Sci. Polym. Symp.* 73:93–98.
- Doi, M., and S. F. Edwards. 1986. *The Theory of Polymer Dynamics*. Clarendon, Oxford.
- Edwards, S. F. 1967. *Proc. Phys. Soc.* 92:9–13.
- Elson, E. L. 1988. Cellular mechanics as an indicator of cytoskeletal structure and function. *Annu. Rev. Biophys. Chem.* 17:397–430.
- Ferry, J. D. 1980. *Viscoelastic Properties of Polymers*. John Wiley, New York.
- Furukawa R., R. Kundra, and M. Fechheimer. 1993. Formation of liquid crystals from actin filaments. *Biochemistry*. 32:12346–12352.
- Graessley, W. W. 1980. Some phenomenological consequences of the Doi-Edwards theory of viscoelasticity. *J. Polym. Sci.* 13:27–34.
- Hendricks, J., T. Kawakatsu, K. Kawasaki, and W. Zimmermann. 1995. On confined semiflexible polymer chains. *Physiol. Rev. E*. 51:2658–2661.
- Ishijima, A., T. Doi, K. Sakurada, and T. Yanagida. 1991. Sub-picowatt force fluctuations of actomyosin in vitro. *Nature*. V352:301–306.
- Janmey, P. A., U. Euteneuer, P. Traub, and M. Schliwa. 1991. Viscoelastic properties of vimentin compared with other filamentous biopolymer networks. *J. Cell Biol.* 113:155–160.
- Janmey, P. A., S. Hvidt, J. Käs, D. Lerche, A. Maggs, E. Sackmann, M. Schliwa, and T. P. Stossel. 1994. The mechanical properties of actin gels. *J. Biol. Chem.* 269:32503–32513.
- Janmey, P. A., J. Peetermans, K. S. Zaner, T. P. Stossel, and T. Tanaka. 1986. Structure and mobility of actin filaments as measured by quasielastic light scattering, viscometry, and electron microscopy. *J. Biol. Chem.* 261:8357–8362.
- Käs, J., L. E. Laham, D. K. Finger, and P. A. Janmey. 1994. Solution ATP affects the bending elasticity of actin filaments implying a low affinity ATP-binding site on F-actin. *Mol. Biol. Cell.* 5:157a.
- Käs, J., H. Strej, M. Bärman, and E. Sackmann. 1993. Direct measurement of the wave-vector-dependent bending stiffness of freely flickering actin filaments. *Europhys. Lett.* 21:865–870.
- Käs, J., H. Strej, and E. Sackmann. 1994. Direct visualization of reptation for semiflexible actin filaments. *Nature*. 368:226–229.
- Kaufmann, S., J. Käs, W. H. Goldmann, E. Sackmann, and G. Isenberg. 1992. Talin anchors and nucleates actin filaments at lipid membranes—a direct demonstration. *FEBS Lett.* 314:203–205.
- Keep, G. T., and R. Pecora. 1985. Reevaluation of the dynamic model for rotational diffusion of thin, rigid rods in semidilute solution. *Macromolecules*. 18:1167–1173.
- Khokhlov, A. R., and A. N. Semenov. 1982. Susceptibility of liquid-crystalline solutions of semiflexible macromolecules in an external orientational field. *J. Physiol. A*. 15:1361–1367.
- Landau, L. D., and E. M. Lifshitz. 1980. *Statistical Physics*, 3rd Ed, Part 1. Pergamon, Oxford.
- Lodge, T. P., N. A. Rotstein, and S. Prager. 1990. Dynamics of entangled polymer liquids: do linear chains reptate? *Adv. Chem. Phys.* 79:1–132.
- Magda, J. J., H. T. Davis, and M. Tirrell. 1986. The transport properties of rod-like particles via molecular dynamics. I. Bulk fluid. *J. Chem. Phys.* 85:6674–6685.
- Mogilner, A., and G. Oster. 1995. The force of actin polymerization. *Science*. submitted.
- Müller, O., H. E. Gaub, M. Bärman, and E. Sackmann. 1991. Viscoelastic moduli of sterically and chemically cross-linked actin networks in the dilute to semidilute regime—measurements by an oscillating disk rheometer. *Macromolecules*. 24:3111–3120.
- Muthukumar, M., and S. F. Edwards. 1983. Screening of hydrodynamic interaction in a solution of rodlike macromolecules. *Macromolecules*. 16:1475–1478.
- Odijk, T. 1983. On the statistics and dynamics of confined or entangled stiff polymers. *Macromolecules*. 16:1340–1344.
- Odijk, T. 1986. Translational friction coefficient of hydrodynamically screened rodlike macromolecules. *Macromolecules*. 19:2073–2074.
- Onsager, L. 1949. The effects of shape on the interaction of colloidal particles. *Ann. N.Y. Acad. Sci.* 51:627–659.
- Perkins, T. T., D. E. Smith, and S. Chu. 1994. Direct observation of tube-like motion of a single polymer chain. *Science*. 264:819–822.
- Prochniewicz, E., Q. Zhang, P. A. Janmey, and D. D. Thomas. 1995. Cooperativity in F-actin: binding of gelsolin at the barbed end affects the structure of the whole filament. *Biophys. J.* 68:A248.
- Radzhivsky, L., and E. Frey. 1993. Kinetic theory of flux-line hydrodynamics: liquid phase with disorder. *Physiol. Rev. B*. 48: 10357–10381.
- Ruddies, R., W. H. Goldmann, G. Isenberg, and E. Sackmann. 1993. The viscoelasticity of entangled actin networks: the influence of defects and modulation by talin and vinculin. *Eur. Biophys. J.* 22:309–322.
- Sackmann, E. 1994. Intracellular and extracellular macromolecular networks—physics and biological function. *Macromol. Chem. Phys.* 194: 7–28.
- Sato, T., Y. Takada, and A. Teramoto. 1991. Dynamics of stiff-chain polymers in isotropic solution. 3. Flexibility effect. *Macromolecules*. 24:6220–6226.
- Schmidt, C. F., M. Bärman, G. Isenberg, and E. Sackmann. 1989. Chain dynamics, mesh size, and diffusive transport in networks of polymerized actin. A quasielastic light scattering and microfluorescence study. *Macromolecules*. 22:3638–3649.
- Semenov, A. N. 1986. Dynamics of concentrated solutions of rigid-chain polymers. Part 1. Brownian motion of persistent macromolecules in isotropic solution. *J. Chem. Soc. (Faraday 2)*. 82:317–329.
- Smith, B. S., L. Finzi, and C. Bustamente. 1992. Direct mechanical measurements of the elasticity of single DNA molecules by using magnetic beads. *Science*. 258:1122–1126.
- Stossel, T. P. 1993. On the crawling of animal cells. *Science*. 260: 1086–1094.
- Suzuki, A., T. Maeda, and T. Ito. 1991. Formation of liquid crystalline phase of actin filament solutions and its dependence on filament length as studied by optical birefringence. *Biophys. J.* 59:25–30.
- Volkmuth, W. D., and R. H. Austin. 1992. DNA electrophoresis in micro-lithographic arrays. *Nature*. 358:600–602.
- Vroege, G. J., and H. N. W. Lekkerkerker. 1992. Phase transitions in lyotropic colloidal and polymer liquid crystal. *Rep. Prog. Phys.* 55: 1241–1315.
- Vroege, G. J., and T. Odijk. 1988. Induced chain rigidity, splay modulus, and other properties of nematic polymer liquid crystals. *Macromolecules*. 21:2848–2858.
- Williams, D. R. M., and M. Warner. 1990. Statics and dynamics of hairpins in worm-like main chain nematic polymer liquid crystals. *J. Physiol. (Paris)*. 51:317–339.